analytical chemistry

Article

pubs.acs.org/ac

Mapping Pixel Dissimilarity in Wide-Field Super-Resolution Fluorescence Microscopy

Cyril Ruckebusch,*[,†] Romain Bernex,[†] Franco Allegrini,[†,‡] Michel Sliwa,[†] Johan Hofkens,[§] and Peter Dedecker[§]

[†]Université de Lille Sciences et technologies, LASIR CNRS, 59655 Villeneuve d'Ascq cedex, France

[‡]Departamento de Química Analítica, Facultad de Ciencias Bioquímicas y Farmacéuticas, Universidad Nacional de Rosario, Instituto de Química de Rosario (IQUIR-CONICET), Suipacha 531, Rosario S2002LRK, Argentina

[§]Department of Chemistry, KU Leuven, Celestijnenlaan 200F, 3001 Heverlee, Belgium

Supporting Information

ABSTRACT: Recent advances in fluorescence bioimaging with single-molecule sensitivity have relied on the analysis and visualization of single-molecule data obtained on smart fluorophores. We describe an alternative method to enhance the information content of densely labeled fluorescence images. Visualization is improved by representing pixels as the dissimilarities of the fluctuations of the fluorescence signals, with the dissimilarity being taken to the mean of the signals over all the pixels. Mapping pixel dissimilarity (Mappix) results in signal and information enhancement of the output images. In addition, the spatial distribution of the fluorescence brightness of the original image is not skewed. This allows large differences of molecular brightness to be handled which turns out to be critical to the fidelity of the final image. In this work, we provide testing of the Mappix approach with both simulated and real data. The results obtained on HEK cells expressing Dronpa photoswitchable fluorescent protein show that, for densely labeled samples, improvement can be obtained on fluorescence images allowing the observation of structural information. Despite some limitations, comparison to state of art methods reveals that Mappix can be very useful for biological imaging applications.

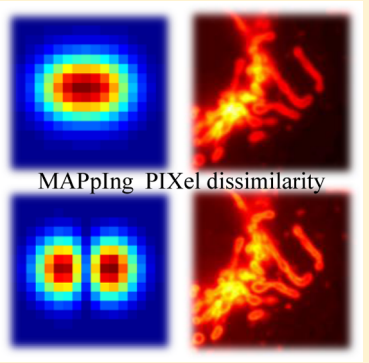

Fluorescence imaging is a major analytical technique for investigating molecular structures. However, the resolution of conventional microscopy is limited by the optical diffraction limit. Functional subdiffraction fluorescence microscopy is based on the use of smart probes that can be switched between two different states (an emissive "on" state and a nonemissive "off" state).[1] Functional super-resolution can be achieved by different subdiffraction imaging techniques, providing insight into biological cellular structures. We refer to refs 2 and 3 for recent reviews. Among these techniques are the so-called deterministic super-resolution techniques such as STimulated Emission Depletion (STED),[4] REverSible Optically Linear Fluorescence Transitions microscopy (RESOLFT),[5−7] Non-linear Structured Illumination Microscopy (NSIM),[8] and Image Scanning Microscopy (ISM).[9] These techniques combine targeted illumination and the properties of the fluorophores to achieve a spatial resolution below the diffraction limit.

Another group of methods is composed of the so-called stochastic super-resolution techniques. These are wide-field techniques which employ the single-molecule nature of fluorescence emission signals. These signals usually rely on the stochastic and sparse activation of individual fluorophores within a sample, and their observation over thousands of frames. The most straightforward approach for data analysis is to perform localization of single emitters by fitting a two-dimensional Gaussian Point Spread Function (PSF) to individually resolved emitters, provided that the distribution of the active emitters in each frame is sufficiently sparse.[10] The localization process is repeated over all the frames, and the resulting positions are summed up to form the super-resolution image of the sample. Single-molecule localization is the building block of many stochastic methods such as STochastical Optical Reconstruction Microscopy (STORM)[11] and PhotoActivation Localization Microscopy (PALM).[2,3,12] Typically, a large improvement can be obtained when emitters are individually resolved, reaching in the best case a resolution down to a few tens of nanometer. However, the underlying requirement for a low density of active fluorophores, low enough to avoid emitter overlap within a single frame, goes along with some limitations for live cell biological applications.

Several approaches, such as multiple-Gaussian model-fitting, have recently been developed.[13,14] Still, the reliability and computational cost can be questioned compared to single-emitter localization routines. A strategy based on subtraction of consecutive images was established,[15] and even though this method has some limitations (e.g., for emitters that remain activated during a series of several frames), the principle of

Received: November 17, 2014
Accepted: April 6, 2015
Published: April 6, 2015

DOI: 10.1021/ac504295p
Anal. Chem. 2015, 87, 4675−4682

applying localization procedures on preprocessed data rather than directly on raw data was demonstrated. Alternatively, a Bayesian approach based on probability maps was proposed.[16] However, the development of methodologies capable of handling image data with density of emitters high-enough to provide reliable structural content is still a main issue in super-resolution fluorescence imaging.[17]

Contrary to localization procedures, some methods rely on statistical analysis of the fluorescence fluctuations in each pixel to extract information on the dynamics of the sample, *e.g.,* Spatiotemporal Image Correlation Spectroscopy (STICS).[18] Another example is Super-resolution Optical Fluctuation Imaging (SOFI),[19,20] which achieves a subdiffraction resolution for densely labeled structures. SOFI uses higher-order statistics by computing temporal cumulants of the blinking fluorescence signal detected in each pixel, and is the best known super-resolution fluorescence correlation method until now. SOFI is compatible with a wide range of imaging modalities and blinking conditions, and remarkably, the resolution enhancement is theoretically unlimited. However, SOFI is a PSF-enhancement method, and with increasing order of SOFI calculation, the brightness of each emitter enters the final SOFI image with the n^{th} power. If the emitters display a range of different brightness, this results in a skewing of the emitter contributions which complicates image representation and hampers interpretation of the samples.

We propose an alternative approach for processing the fluorescence fluctuations present in fluorescence imaging with single-molecule sensitivity. This approach relies on the evaluation of the dissimilarity of the pixel signal to the average signal over all the pixels, resulting in pixel-dissimilarity representations of the images. Intuitively, dissimilarity can be understood as a measure of both the correlation and the distance between two signal vectors. In the literature, different criteria were used to evaluate the (dis)similarity between signals[21] with the common general idea to emphasize characteristics which are difficult to evaluate in statistical approaches, such as shape or mutual resemblance. In this work, dissimilarity is being estimated by adapting a criterion that was originally developed for the resolution of spectroscopic mixtures, where very similar spectral shapes are usually observed.[22] The advantage of this approach is that the intensity of detector pixels that observe emission from overlapping emitters localized in neighboring pixels will be strongly reduced, aiding in discriminating between adjacent emitters. Consequently, Mapping pixel dissimilarity (Mappix) yields a contrast enhancement and can resolve emitters that are closely spaced below the diffraction limit. Mappix is an image processing enhancement but cannot be considered a sub-diffraction imaging technique as no hard mathematical description of the image can be provided. Comparison between SOFI and Mappix performed on simulated data and on live cells expressing Dronpa photoswitchable fluorescent protein were conducted as a proof of principle. The proposed method is of particular relevance for high-sensitivity imaging of biological cellular structures based on single-molecule fluorescence as the results are more robust on brightness scale and on label density.

MATERIALS AND METHODS

Simulated data. We simulated stochastic fluorescence microscopy data in order to evaluate the proposed method. We placed fluorophores on a regular grid representing the camera pixels. The relative intensity of each of the fluorophores in each pixel was computed by numerically integrating a normal cumulative distribution function with a Full-Width at Half–Maximum (fwhm) of 270 nm over the area of the pixel. The emitters switching between a bright and a dark fluorescent level can be described by a two-state model where $k_{on} = 1/\tau_{on}$ and $k_{off} = 1/\tau_{off}$ are the rate constants from the "on" to "off" and the "off" to "on" states, respectively. The activity of the fluorophores was modeled by a time-continuous Markov process with fixed expected active times of τ_{on} = 2 s and with fixed expected dark times τ_{off} of 0.5 s. These characteristic times were sampled from exponential distributions with the corresponding decay times and were not synchronized with the acquisition time. We assumed an emission of 10000 photons per second for each fluorophore, and a per-frame duration of 1s. To obtain the number of photons emitted by a fluorophore in a specific acquisition frame, the emission rate was multiplied with the time the fluorophore spent in this frame. The number of photons measured in each pixel from a given frame was drawn from a Poisson distribution. The resulting output value of the EMCCD was modeled with a gamma distribution taking a mean gain of 80. Electron noise was added using a Gaussian distribution. Different data sets were simulated generating images of 1000 frames, on a 40*40 pixel-grid with a pixel size of 30 nm. For simulations with two emitters, single emitters were positioned such that the distance between them corresponds to 210 nm. Another situation consisted of nine single emitters regularly positioned either on a circle of 300 nm diameter or on one of 210 nm. Finally, for a simulated system consisting of four equally spaced fluorophores placed along a line, single emitters were positioned such that the distance between two emitters corresponds to 210 nm. In this scenario, the results obtained for two situations are reported. In the first case, the intensity of the overlapping emitters is the same whereas for the second data simulation, the intensity was varied between successive emitters (1, 0.75, 0.5, and 0.25 from left to right, respectively). To vary intensity, a limit was set on the maximum number of photons an emitter can generate.

Live cell preparation. Human embryonal kidney (HEK-293T) cells were cultured in DMEM supplemented with 10% FBS, glutamax, and gentamicin (all GIBCO) on glass-bottom dishes (MatTek). Twenty-four h prior to imaging the cells were transfected with a pCDNA3 plasmid encoding DAKAP-Dronpa using calcium-phosphate mediated transfection. Just prior to imaging, the cells were washed three times with Hank's Balanced Salt Solution (HBSS) and finally imaged at room temperature in 1 mL of HBSS.

Single-molecule fluorescence imaging microscopy. Live-cell imaging experiments were performed on an Olympus Cell*TIRF system, equipped with 488 and 405 nm laser light sources, Olympus 150x NA 1.45 objective, and a Hamamatsu ImageEM electron-multiplied CCD camera. The optical pixel size of the camera was equal to 100 nm.

Cells expressing DAKAP-Dronpa were visualized in epi mode using the 488 nm laser and standard GFP filter sets. The total illumination power was adjusted to approximately 1–2 mW as measured immediately above the objective when the sample was removed.

For each cell approximately 1000 images were acquired using a per-frame exposure time of 33 ms. The electron-multiplication gain of the camera was set at approximately 300 (as defined by the manufacturer).

DOI: 10.1021/ac504295p
Anal. Chem. 2015, 87, 4675–4682

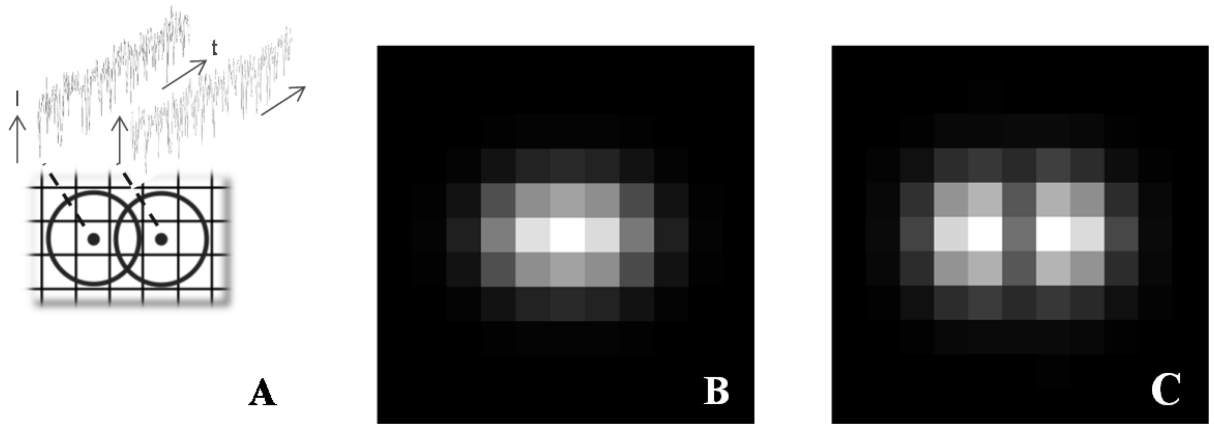

Figure 1. Principle of Mappix, based on the evaluation and mapping of pixel-dissimilarity values for single-molecule sensitive fluorescence imaging. (A) Signals from two neighboring emitters separated by a distance of two pixels recorded on pixels of a CDD camera. Each pixel contains a trace of the fluorescence intensity fluctuations over time. (B) Original image. White pixels correspond to bright signals. (C) Image obtained mapping pixel-dissimilarity values. Dark pixels correspond to low dissimilarity. A vertical separation between the two emitters is observed which results in the separation of two emission sources. Two emitters can be detected as long as the distance between them is larger than 1.5 times the size of a pixel.

Pixel dissimilarity. Single-molecule sensitive fluorescence microscopy provides data consisting of a stack of K frames where K can be up to several thousands. Each frame contains $n \times n$ pixel intensity values. The signal associated with each pixel i is considered a (pixel-)vector $\mathbf{p_i}$ of size K containing the fluorescence intensities acquired along the measurement time. The mean of all the pixel-vectors $\mathbf{p_i}$ is denoted $\mathbf{r}$ and is normalized to unit length.

The (dis)similarity between two objects measures the (in)dependency between the sequence of measurements representing these objects. It can be estimated in many ways that are based on correlation or/and on distance. In this work, the dissimilarity d_i is defined as the cross product of the pixel-vector $\mathbf{p_i}$ and the mean taken over all the pixel vectors, $\mathbf{r}$, as in eq 1.

$$d_i = \mathbf{p_i} \times \mathbf{r} = \|\mathbf{p_i}\| \|\mathbf{r}\| \sin \alpha_i \quad (1)$$

where the notation ||...|| corresponds to the vector norm taken in the time dimension of the signal (it is recalled that $\|\mathbf{r}\| = 1$) and α_i is the angle between the pixel-vector and the mean vector. We make use here of the fact that computing the cross product between two vectors can be performed easily as a determinant of a square matrix (details are given in the Supporting Information).

One can intuitively understand the way signal dissimilarity is evaluated from the geometric meaning of the cross product. The magnitude of the cross product can be interpreted as the positive area of the parallelogram having $\mathbf{p}$ and $\mathbf{r}$ as sides. This value tends toward zero when the two vectors have the same direction or when one of the two vectors is of zero length. The larger the angular difference between the vectors $\mathbf{p}$ and $\mathbf{r}$, and the larger the norm of the signal vector (the brighter the pixel), the higher the dissimilarity value. In addition, one can directly infer from eq 1 that assuming a constant value of the angle α between the two vectors, the pixel fluorescence brightness enters the calculation of the dissimilarity linearly.

Conversely, and more interestingly for the purpose of this work, low dissimilarity values may be observed for two distinct situations. The first is, obviously, for pixels of very small signal (noise). The second is of greater interest for signal enhancement in the context of single-molecule sensitive fluorescence microscopy. It corresponds to very similar pixel-signal $\mathbf{p}$ and mean vector $\mathbf{r}$. This can be observed for pixels that contain contributions from multiple emitters (these pixels approximate the mean vector). As a result, the Mappix intensity is reduced for pixels that detect overlapping fluorescence from different emitters.

Mappix images. A schematic overview of the Mappix method is provided in Figure 1 showing a conceptual experiment involving two fluctuating fluorophores spaced closely together. Due to the fluctuating nature of the emitters, each detector pixel reports varying fluorescence levels in time (Figure 1A). These values provide the components of the pixel-vectors $\mathbf{p}$. The magnitude of these vectors corresponds to the average pixel intensity. The original image that would correspond to the average of the movie data is shown in Figure 1B. The results that are obtained calculating pixel-dissimilarity are shown in Figure 1C. For bright pixels in Figure 1B, i.e. where the emissions of the two emitters overlap, small dissimilarity values are returned in Figure 1C resulting in the separation of two highly overlapping emitters.

Mappix is a pixelated method and, as such, it is limited by the finite optical size of the camera pixels. Two emitters can be distinguished providing that they are separated by a distance corresponding to at least 1.5 pixels even in situations where their individual emission can hardly be selectively observed in time. However, it should be noted that where signals overlap, the shape of the processed signal is changed and cannot anymore be approximated by a sum of Gaussian PSF.

Mappix images can be estimated considering full movie data (K frames) or repeating the procedure for shorter image sequences. In the latter case, multiple images are output and the results are averaged to produce the final Mappix image. For a short image sequence, dissimilarity is calculated in reference to the mean taken over the images composing the sequence. This enables correcting for dynamic variation of the signal that may occur at longer time scale than the fluctuations of the single emitters. The choice of the number of frames per sequence is data-dependent and is discussed in the Supporting Information. Typically, good results can be obtained considering a few tens of frames on movies consisting of a thousand images.

In addition, Mappix images can be calculated for the full image (all the pixels) or locally for patches of the full image. As for shorter image sequences, pixel dissimilarity differences are

DOI: 10.1021/ac504295p
Anal. Chem. 2015, 87, 4675−4682

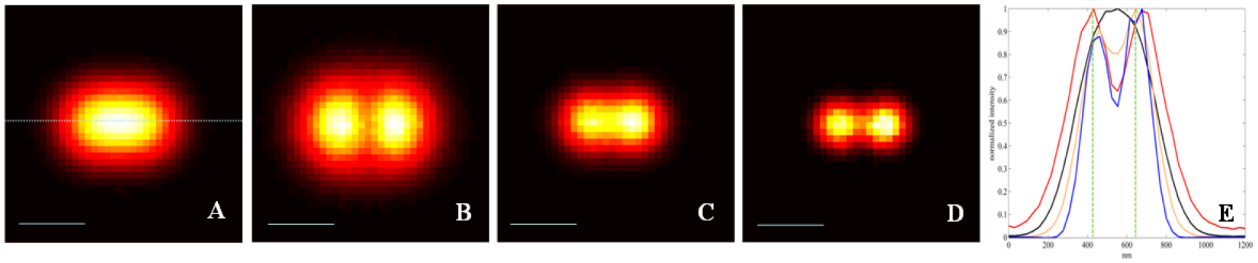

Figure 2. Comparison of the results obtained by Mappix and SOFI on simulated data. (A) Original image corresponding to two neighboring emitters separated by 210 nm for a PSF of 270 nm (fwhm). (B–D) Images obtained from the application of Mappix, 2nd-order SOFI, and 3rd-order SOFI, respectively. (E) Normalized intensity profiles extracted from the dotted line drawn in part A. Black solid line corresponds to the signal of the original image, red solid line to Mappix, orange and blue solid lines to 2nd-order and 3rd-order SOFI, respectively. Scale bar: 300 nm.

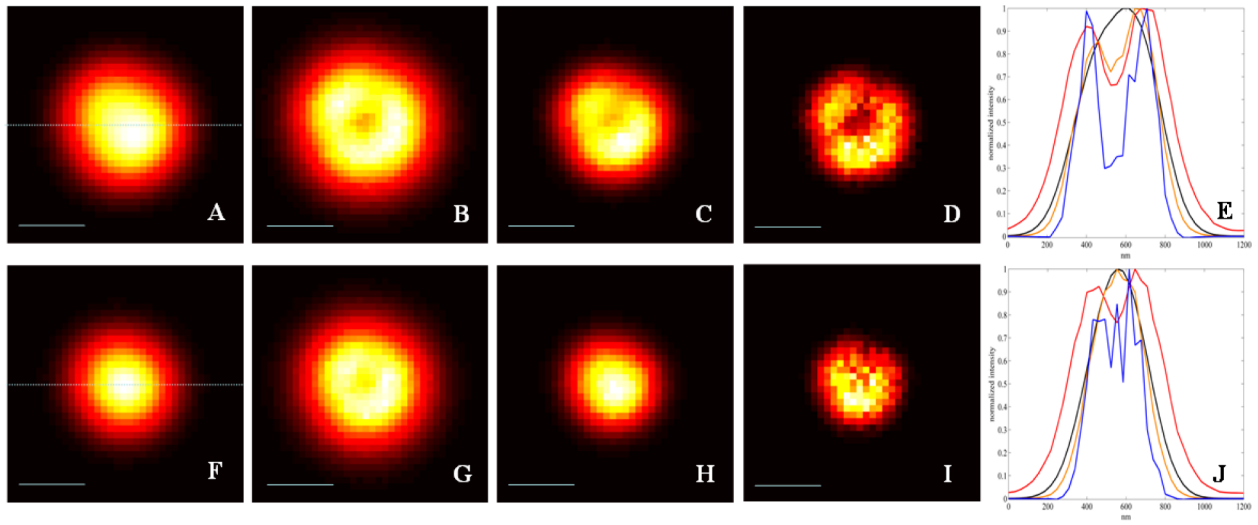

Figure 3. Comparison of the results obtained by Mappix and SOFI on simulated data. (A) Original image corresponding to nine single emitters (PSF of 270 nm fwhm) regularly positioned on a circle of 300 nm diameter. (B–D) Images resulting from the application of Mappix, 2nd-order SOFI, and 3rd-order SOFI, respectively. (E) Normalized intensity profiles extracted from the dotted line in part A. (F) Original image obtained for a circle of 210 nm diameter. (G–I) Mappix, 2nd-order SOFI, and 3rd-order SOFI images, respectively. (J) Normalized intensity profiles extracted from the dotted line in part F. Color code in parts E and J: black solid line corresponds to the signal of the original image, red solid line to Mappix, orange and blue solid lines to 2nd-order and 3rd-order SOFI, respectively. Scale bar: 300 nm.

highlighted when a smaller spatial area is considered. However, attention should be paid to the fact that the mean vector is different for each patch. The calculation of many local patches, and their combination into a larger output images, might be envisaged. However, it should be noted that the final image might be affected by the fact that dissimilarity is assessed to different mean vectors. This approach was not explored further in this work.

The routines used for Mappix were written in MATLAB version 7.4.0 (R2007a) or higher.[23] These routines are available on request to the authors. SOFI images were obtained using Localizer,[24] a freely available and open source software package that implements the computational data processing inherent to several types of super-resolution fluorescence imaging.

RESULTS AND DISCUSSION

The ability of stochastic super-resolution methods to resolve structural features depends on the labeling density and on the potential to separate the emission of individual fluorophores in time.[25] A high value of the ratio of "off"- and "on"-switching of the fluorophores, i.e., a τ_{off} much longer than the τ_{on}, is crucial for successful localization. As reported in the literature, a ratio in the vicinity of 1000 is required for the separation of two adjacent filaments separated by 30 nm using the STORM localization procedure (for fluorophores positioned every 8.5 nm).[26] On the contrary, in the current work, the possibility to improve the detection and the visualization of labeled structures for which this ratio is much smaller in investigated. It should be clear that single-molecule localization procedures cannot be applied in these conditions as there always exists more than one active emitter at the same time in a diffraction limited area.

Simulations. Figure 2 reports the results obtained on simulations of two single emitters that are separated by a distance of 210 nm. This situation corresponds to a distance shorter than the diffraction limit. These emitters are blinking stochastically with a "on"-to-"off" ratio of 0.25 and exhibit a τ_{off} value two times shorter than the acquisition time. The results obtained by applying Mappix (see Figure 2B) are reported along the ones provided by SOFI using second- and third-order cumulants (see Figure 2C and Figure 2D, respectively). First, it can be noted that all the images display a clear enhancement of the structural information and imaging details. Clearly, for SOFI, some resolution improvement is observed in particular for third-order SOFI, for which the best results are obtained. From the profiles in Figure 2E, it is observed that the contrast for the Mappix image is the same as for the third-order SOFI image providing good separation of the two sources.

DOI: 10.1021/ac504295p
Anal. Chem. 2015, 87, 4675–4682

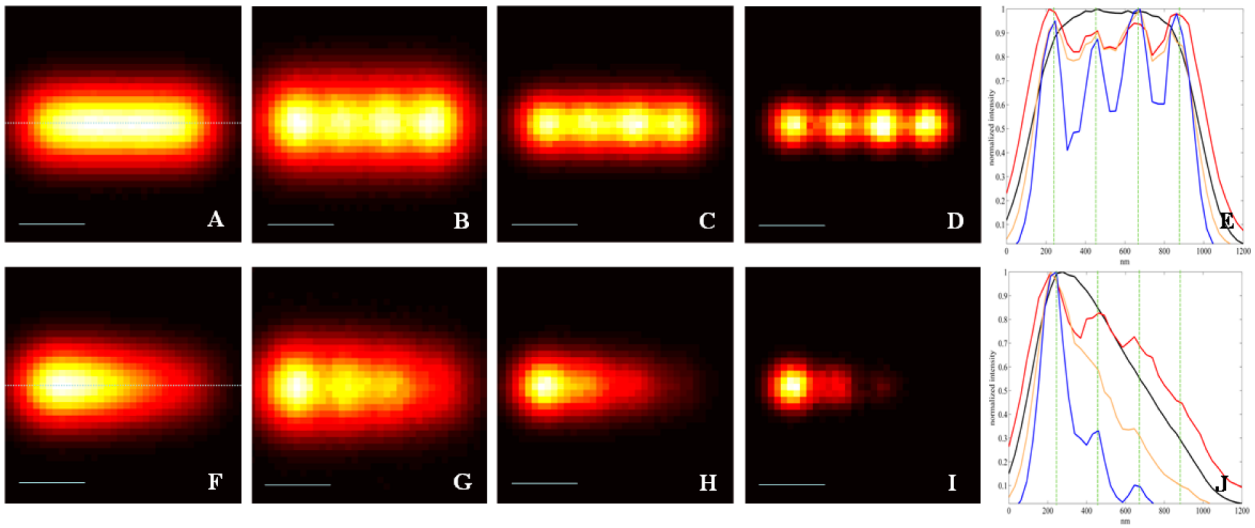

Figure 4. Comparison of the results obtained by Mappix and SOFI on simulated data. (A) Original image corresponding to four neighboring emitters of the same intensity separated by 210 nm for a PSF of 270 nm (fwhm). (B–D) Images resulting from the application of Mappix, 2nd-order SOFI, and 3rd-order SOFI, respectively. (E) Normalized intensity profiles extracted from the dotted line in part A. (F) Original image corresponding to four neighboring emitters with intensity ratio 1, 0.75, 0.5, and 0.25. (G–I) Mappix, 2nd-order SOFI, and 3rd-order SOFI images, respectively. (J) Normalized intensity profiles extracted from the dotted line in part F. Color code in parts E and J: black solid line corresponds to the signal of the original image, red solid line to Mappix, orange and blue solid lines to 2nd-order and 3rd-order SOFI, respectively. Scale bar: 300 nm.

From the results in Figure 2, the conceptual difference between Mappix and SOFI can be discussed further. Mappix is a signal processing approach that can help reveal structural features (separating two neighboring emitters). However, contrary to SOFI, Mappix does not provide any enhancement of the PSF of individual emitters. Consequently, no theoretical resolution enhancement can be obtained for Mappix, as observed comparing the respective size of the images in Figures 2A and 2B. Still information about the underlying structure is revealed due to the fact that for pixels with overlapping PSFs, lower dissimilarity values are returned on the image. Mappix, provides separation of the sources and the presence of two emitters can be detected as long as there are intermediate pixels present between their centers. By comparison, for SOFI, the computation of the n^{th}-order cumulant theoretically generates an image in which the resolution is theoretically enhanced by a factor $\sqrt{n}$ for a Gaussian PSF.[19] Lastly, it should be noted that although detection and separation of two emitters is still possible in situations where strong emission overlap exists, Mappix should not be applied to determine the position of these emitters as the calculation of dissimilarity results in distortion of the PSF signal of individual emitters.

To elaborate further on the potential of Mappix to recover some structural information in dense labeling conditions and unfavorable blinking characteristics, the results obtained for a simulation involving a structure of nine single emitters are reported in Figure 3. These emitters are regularly positioned on a circle and have the same blinking characteristics as in the previous example. A representative fragment of the movie data is provided as Supporting Information. No structure can be observed as the nine emitters are confined in a diffraction limited area. In Figures 3A–E, the results corresponding to a 300 nm diameter circle are shown. From the images and Figure 3E, it can be observed that the three approaches are capable of restoring the appropriate structural information (a donut-like intensity distribution), the best resolution being achieved by third-order SOFI, despite some distortion of the intensity distribution. Mappix and second-order SOFI are doing equally well in terms of contrast and intensity distribution. However, contrary to SOFI, Mappix does not provide PSF enhancement as already mentioned and, therefore, we would recommend the application of SOFI in this situation.

Interestingly, when the same situation but for a 210 nm diameter circle is investigated, the conclusions are different. In Figure 3F, the original image is shown. The Mappix image is shown in Figure 3G and SOFI images are provided in Figures 3H and 3I. The profiles obtained from these images are compared in Figure 3J. For SOFI, whatever the order of the cumulant, no structural information can be observed, likely due to incomplete convergence of the calculated cumulants. On the contrary, the spatial distribution of the intensity corresponding to the simulated structure can still be identified from the Mappix image. These results obtained on simulated data enable to highlight one of the striking features of the Mappix approach which is that it can still provide structural information in labeling and blinking conditions where, to our knowledge none of the state of art methods can be applied.

As shown in Figure 4, the results obtained on simulations of four equally spaced fluorophores that are separated by a distance of 210 nm are now reported. For the simulated data shown in Figure 4A, the intensity of the emitters is the same whereas for the ones in Figure 4F, intensity was varied between successive emitters, decreasingly from left to right. The results obtained by applying Mappix (see Figures 4B and 4G) are reported together with the ones provided by SOFI using 2nd- and third-order cumulants (see Figures 4C and 4H, and Figures 4D and 4I, respectively). In a first instance, it can be noted that the images display a clear enhancement of the imaging details, including the Mappix images. To further compare the different images, Figures 4E and 4J show the line profiles through the PSF of the four emitters for the two situations. The profiles reported in Figure 4E highlight the ability of the different methods to separate the four neighboring overlapping emitters of the same intensity. As can be observed, Mappix provides images with an information gain comparable to second-order

DOI: 10.1021/ac504295p
Anal. Chem. 2015, 87, 4675–4682

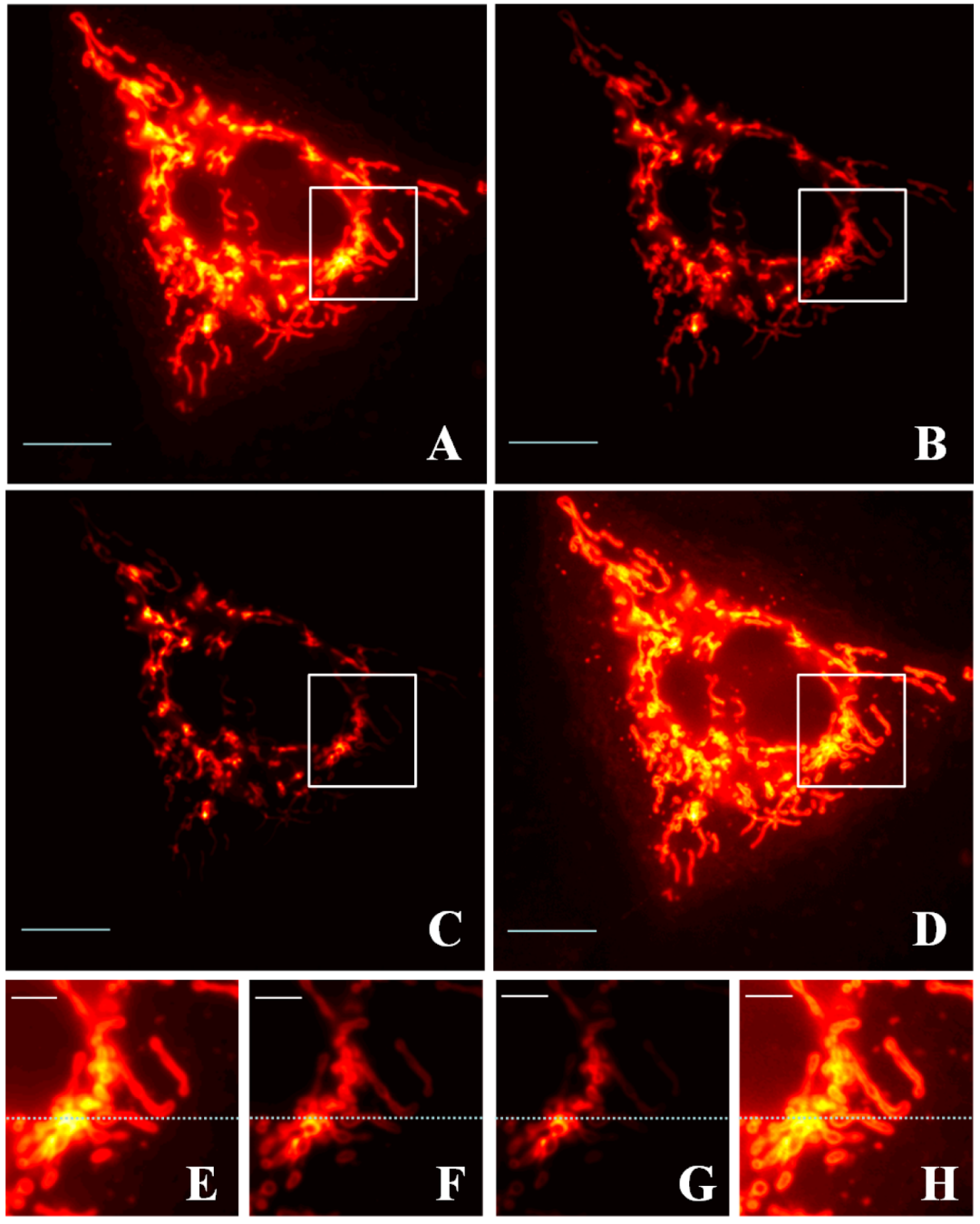

Figure 5. Live-cell image of HEK293-T cell labeled expressing DAKAP-Dronpa visualized in the Epi-illumination mode. (A) Original wide-field image generated by averaging all the frames of the acquired movie (1000 frames, 30 ms per frame). (B and C) 2nd-order SOFI and 3rd-order SOFI images, respectively. (D) Mappix image obtained averaging the results obtained on the 10-frames sequence. (E–F) Magnified views of the box marked on images A–D, respectively. Scale bars: A–D: 10 μm, E–H: 2 μm.

SOFI in terms of emitter separation. Applying third-order SOFI, the resolution improvement is better in this situation.

When individual emitters have fairly different intensities, the situation depicted before is changed, as shown from the intensity profiles reported in Figure 4J. For SOFI intensity, a severe brightness skewing of the emitter contributions is obtained because the brightness is raised to the power n for n^{th}-order SOFI calculation. This may lead to distortion of the results. This effect can be observed on the results provided in Figures 4H and 4I. The contributions of the dimmer emitters are masked by the signal of the brighter ones. For second-order SOFI, the presence of the rightmost emitter can hardly be detected on the image because the local contrast is poor. For third-order SOFI, despite some theoretically improvement in spatial resolution, the situation is worse. On the contrary, the red profiles depicted in Figure 4J based on the intensity of the Mappix image in Figure 4G allow for the detection of the presence of four emitters. A clear information enhancement is obtained compared to the original. For Mappix results, the fidelity of the relative intensity distribution on the final image approximates that of the unprocessed data better. In the presence of large brightness scaling, as for the simulation, this may result in a better efficiency to detect overlapping emitters, and to discriminate them.

DOI: 10.1021/ac504295p
Anal. Chem. 2015, 87, 4675–4682

The development of high-sensitivity methods based on single-molecule fluorescence for imaging biomolecules in living cells requires advances for situations in which the labeling density is high. This is true for all super-resolution techniques as the resolution is directly related to the label density by the Nyquist-Shannon sampling theorem. In addition, quantitative processing requires that attention should be paid to the robustness of the method with respect to brightness distribution of the fluorophores.[27]

Live-cell imaging experiment with HEK293-T cells expressing Dronpa targeted to the mitochondria. Figure 5 provides the results obtained for live-cell imaging experiment with HEK293-T cells expressing Dronpa targeted to the mitochondria. Figure 5A shows the original image. A representative fragment of the movie data is provided as Supporting Information. As this fragment clearly shows, the active Dronpa fluorophores are present in very high density in each frame necessitating an analysis strategy capable of adapting to these conditions.

Figures 5B and 5C show the results for second- and third-order SOFI, respectively. Background elimination is obtained and an improvement in the spatial resolution is observed. However, because of the large dynamic range of the intensity signal which may result from nonuniform illumination of the sample and possible brightness heterogeneity of the fluorophores, the SOFI images are difficult to visualize directly. This is especially noticeable in the third-order SOFI image where extracting full spatial information is difficult (see Figure 5C) if the color mapping is scaled to the full range of intensities. Even for second-order SOFI, this trend is already evident in the large dynamic range of the signal.

The results obtained with the Mappix approach are provided in Figure 5D. By comparison to second-order SOFI, the main observation is that, overall, the dynamic range of the original image is preserved. This allows for the observation of the full cell structure despite strong brightness scaling of the original image. In addition, compared to the original image, the cellular structure is more readily observable in the Mappix data, as shown in the magnified views in Figure 5E and in Figure 5H. In Figure 6, intensity cross sections of the images provided in Figures 5E–H are provided. Despite the large dynamic range in the original image, local contrast enhancement and local detail can be observed for Mappix (see Figure 6, red profile) when these profiles are compared.

The results shown for Mappix in Figure 5D were obtained by averaging 10-frames sequences to produce the final image. The choice of the number of frames per sequence is data-driven and thus related to experimental parameters such as the blinking characteristics of the fluorophores, the presence of stationary background, autofluorescence, bleaching, etc. Typically, according to our experience on different data sets, considering ten to a few tens of frames per sequence provide good quality results. However, this choice is left to the user. In the Supporting Information, the results obtained on HEK293-T with a number of frames per subset varying from 1000 (full sequence) down to 10 are reported. When considering the full sequence of frames, pixel-dissimilarity is taken over the overall mean-pixel signal. In this way, stationary background can be accounted for, as for SOFI. However, compared to the original image, the information gain remains limited, as observed in Figure S1. Another alternative is to process multiple sequences of a limited number of frames and to average the obtained results. To illustrate this, the images obtained for 10- and 50-frames per subset of the full sequence movie are provided in Figures S1A and S1B, respectively. Considering multiple subsequences of the full movie allows handling dynamic variations of the signals, i.e variations which evolve at longer time scale than the fluorescence signal of the single emitters. Bleaching is an example. As observed from the profiles in Figure S1E, the results obtained from multiple subsequences show some resolution improvement that provides a better distinction of the features of the biological structure, despite that static background is not handled by the procedure in this case. However, this is not really an issue as background could be handled in other ways. In our opinion, the fact that the choice of the number of frames per subset of the full sequence is made by the user should not be considered a limitation but a way to adapt to the many possible different characteristics of the raw data in smart-fluorophore imaging.

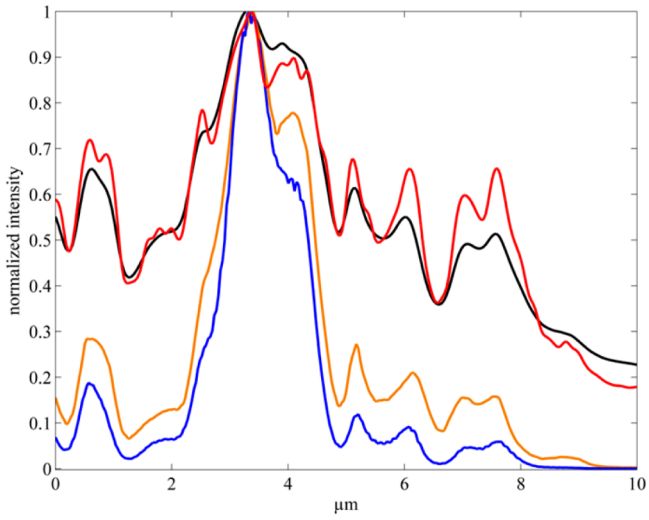

Figure 6. Normalized intensity profiles extracted from the dotted line in Figures 5E–H provided for contrast comparison. Black solid line corresponds to the signal of the original image, red solid line to Mappix, orange and blue solid lines to 2nd-order and 3rd-order SOFI, respectively.

It should be noted that the results provided in Figure 5 were obtained without performing any pre- or postprocessing of the raw super-resolution data. More specifically, no background correction method was applied, nor was it corrected for offset or was intensity scaling performed. This can be observed on the profiles in Figure 6 which are compared directly to the original image signal. The choice to report raw data for Mappix results was made in order to avoid any biased interpretation of the images provided. It has recently been acknowledged in the literature that the quality of the processed image can be determined by the choice of the background correction algorithm to a large extent.[28] Still, it is worth mentioning that Mappix can be applied in combination with any type of image pre- or postprocessing. As for Mappix results, no image enhancing technique was applied to the images obtained using SOFI.

In Supporting Information, additional results obtained applying Mappix to live HEK293-T cells expressing a construct encoding Dronpa targeted to the plasma membrane are reported on.[29] As previously, the results are compared with SOFI (see Figure S2). For these data corresponding to dense labeling conditions, histograms of pixel intensity are provided in Figure S3. This enables highlighting how the Mappix approach

DOI: 10.1021/ac504295p
Anal. Chem. 2015, 87, 4675–4682

preserves information about the overall intensity distribution on the original image better.

CONCLUDING REMARKS

We demonstrated that an approach based on pixel dissimilarity, for which the name Mappix was proposed, can be a powerful alternative for processing densely labeled data in fluorescence images with single-molecule sensitivity. Calculation is uncomplicated, and the method can be applied to a wide range of imaging modalities and any characteristics of the raw data. However, in normal labeling and blinking situations, Mappix yields images with only a relatively moderate improvement and does not perform better than state of art PSF-enhancement methods.

The strength of the Mappix approach is that it is robust to labeling density, blinking characteristics, and brightness variations within the original image. Mappix still provides improved information, enhancing the structural content of the image in situations where other techniques are limited by the fact that the fluorescence emission of an individual fluorophore cannot be separated in time or that the brightness of the original image is skewed. The method may thus provide a useful alternative for some biological imaging applications, where, on the one hand, signal enhancement is aimed for structural analysis and, on the other hand, global contrast preservation is required for functional or quantitative analysis. To conclude, we would recommend using Mappix as an image enhancement technique for visual and semiquantitative inspection of the image data combined with SOFI imaging for subdiffraction imaging.

ASSOCIATED CONTENT

Supporting Information

Additional information as noted in the text. This material is available free of charge via the Internet at http://pubs.acs.org.

AUTHOR INFORMATION

Corresponding Author

*E-mail: cyril.ruckebusch@univ-lille1.fr.

Notes

The authors declare no competing financial interest.

ACKNOWLEDGMENTS

The authors thank Marc Offroy, Simon Stein, and Joerg Enderlein for fruitful discussions. The authors acknowledge the financial support of the Agence National de la Recherche (ANR-14-CE08-0015-01 ultrafast nanoscopy) and of the Programme International de Coopération Scientifique (PICS) between the Centre National de la Recherche Scientifique (CNRS) and the research foundation Flanders (FWO). P.D. is a postdoctoral fellow of the FWO.

REFERENCES

(1) Dedecker, P.; De Schryver, F. C.; Hofkens, J. *J. Am. Chem. Soc.* **2013**, *135*, 2387−2402.
(2) Klein, T.; Poppert, S.; Sauer, M. *Histochem. Cell. Biol.* **2014**, *141*, 561−575.
(3) Sengupta, P.; Van Engelenburg, S. B.; Lippincott-Schwartz, J. *Chem. Rev.* **2014**, *114*, 3189−3202.
(4) Hell, S. W.; Wichmann, J. *Opt. Lett.* **1994**, *19*, 780−782.
(5) Hell, S. W. *Nat. Biotechnol.* **2003**, *21*, 1347−1355.
(6) Dedecker, P.; Hotta, J. I.; Flors, C.; Sliwa, M.; Uji-I, H.; Roeffaers, M. B. J.; Ando, R.; Mizuno, H.; Miyawaki, A.; Hofkens, J. *J. Am. Chem. Soc.* **2007**, *129*, 16132−16141.
(7) Hofmann, M.; Eggeling, C.; Jakobs, S.; Hell, S. W. *Proc. Natl. Acad. Sc. U. S. A.* **2005**, *102*, 17565−17569.
(8) Rego, E. H.; Shao, L.; Macklin, J. J.; Winoto, L.; Johansson, G. A.; Kamps-Hughes, N.; Davidson, M. W.; Gustafsson, M. G. L. *Proc. Natl. Acad. Sci. U. S. A.* **2012**, *109*, E135−E143.
(9) Muller, C. B.; Enderlein, J. *Phys. Rev. Lett.* **2010**, *104*, 198101.
(10) Sabarita, J. B. *Histochem. Cell. Biol.* **2014**, *141*, 587−595.
(11) Rust, M. J.; Bates, M.; Zhuang, X. W. *Nat. Methods* **2006**, *3*, 793−795.
(12) Betzig, E.; Patterson, G. H.; Sougrat, R.; Lindwasser, O. W.; Olenych, S.; Bonifacino, J. S.; Davidson, M. W.; Lippincott-Schwartz, J.; Hess, H. F. *Science* **2006**, *313*, 1642−1645.
(13) Huang, F.; Schwartz, S. L.; Byars, J. M.; Lidke, K. A. *Biomed. Opt. Express* **2011**, *2*, 1377−1393.
(14) Simonson, P. D.; Rothenberg, E.; Selvin, P. R. *Nano Lett.* **2011**, *11*, 5090−5096.
(15) Burnette, D. T.; Sengupta, P.; Dai, Y. H.; Lippincott-Schwartz, J.; Kachar, B. *Proc. Natl. Acad. Sci. U. S. A.* **2011**, *108*, 21081−21086.
(16) Cox, S.; Rosten, E.; Monypenny, J.; Jovanovic-Talisman, T.; Burnette, D. T.; Lippincott-Schwartz, J.; Jones, G. E.; Heintzmann, R. *Nature Meth.* **2012**, *9*, 195−200.
(17) Holden, S. J.; Uphoff, S.; Kapanidis, A. N. *Nat. Methods* **2011**, *8*, 279−280.
(18) Hebert, S.; Costantino, P. W.; Wiseman, P. *Biophys. J.* **2005**, *88*, 3601−3614.
(19) Dertinger, T.; Colyer, R.; Iyer, G.; Weiss, S.; Enderlein, J. *Proc. Natl. Acad. Sci. U. S. A.* **2009**, *106*, 22287−22292.
(20) Mukamel, E. A.; Babcock, H.; Zhuang, X. *Biophys. J.* **2012**, *102*, 2391−2400.
(21) Paclik, P.; Duin, R. P. W. *Real-Time Imaging* **2003**, *9*, 237−244.
(22) Sanchez, F. C.; Toft, J.; Van den Bogaert, B.; Massart, D. L. *Anal. Chem.* **1996**, *68*, 79−85.
(23) MATLAB; The Mathworks Inc.: Natick, Massachusetts, USA.
(24) Dedecker, P.; Duwé, S.; Neely, R. K.; Zhang, J. *J. Biomed. Opt.* **2012**, *17*, 126008.
(25) Lord, J. S.; Lee, H. D.; Moerner, W. E. *Anal. Chem.* **2010**, *82*, 2192−2203.
(26) van de Linde, S.; Wolter, S.; Heilemann, M.; Sauer, M. *J. Biotechnol.* **2010**, *149*, 260.
(27) Yang, Y.; Zhang, C. *Anal. Chem.* **2014**, *86*, 967−972.
(28) Hoogendoorn, E.; Crosby1, K. C.; Leyton-Puig, D.; Breedijk, R. M. P.; Jalink, K.; Gadella, T. W. J; Postma, M. *Sci. Rep.* **2014**, *4*, 3854.
(29) De Rooi, J.; Ruckebusch, C.; Eilers, P. H. C. *Anal. Chem.* **2014**, *86*, 6291−6298.

DOI: 10.1021/ac504295p
Anal. Chem. 2015, 87, 4675−4682